doi:10.3788/gzxb20144311.1105001

二元相位菲涅尔波带片近场俘获高低折射率粒子

赵艳,张耀举,朱艳
(温州大学 物理与电子信息工程学院,浙江 温州 325035)

摘 要:采用双环形涡旋偏振光照射二元相位亚波长菲涅耳波带片的方法,实现了对高低折射率瑞利(Rayleigh)粒子的近场俘获.利用角谱理论计算了菲涅耳波带片的衍射场分布.改变入射光的截断参数(β)和涡旋角(δ),可以在菲涅耳波带片的近场区域产生亮斑和暗斑.计算发现,当 $\beta=1.09$ 和 $\delta=0$ 时,在近场区域产生亚波长三维亮斑,能够稳定俘获 19 nm 的金粒子,金粒子的折射率大于周围介质,轴向和横向俘获距离分别为 0.4921λ 和 0.2844λ.当 $\beta=1.45$ 和 $\delta=0.414\pi$ 时,在近场区域产生光墙包围着的三维暗斑,可以将 30 nm 的空气泡稳定地俘获在暗斑中心,空气泡的折射率小于周围介质的折射率.两种情况计算所得的俘获距离均小于传统远场俘获系统中的距离.该系统可以用来精确俘获两类折射率不同的 Rayleigh 粒子.

关键词:近场俘获;折射率;菲涅耳波带片;瑞利粒子;截断参数
中图分类号:O436.1 **文献标识码**:A **文章编号**:1004-4213(2014)11-1105001-7

Near-field Trapping High and Low Refractive Index Particles with a Binary Phase Fresnel Zone Plate

ZHAO Yan, ZHANG Yao-ju, ZHU Yan
(*College of Physics and Electronic Information Engineering, Wenzhou University, Wenzhou, Zhejiang* 325035, *China*)

Abstract: A method of near-field trapping high and low refractive index Rayleigh particles was proposed using a binary phase Subwavelength Fresnel Zone Plate (SFZP) illuminated by the double-ring-shaped vortex beam. Based on the angular spectrum representation, the distribution of SFZP's diffraction field was calculated. Bright and dark spots can be generated in the near field of the SFZP by changing the truncation parameter (β) and the vortex angle (δ) of the incident beam. Numerical results show that the SFZP can generate a subwavelength three-dimensional (3D) bright spot in the near-field region when $\beta=1.09$ and $\delta=0$. The tiny bright spot can be used to stably trap a gold particle with radius 19 nm, whose refractive index is higher than that of the ambient medium. The axial and transverse trap distances are respective 0.4921λ and 0.2844λ. When $\beta=1.45$ and $\delta=0.414\pi$, a 3D dark spot surrounded by a light shell can be formed in the near-field region. An air bubble with radius 30 nm is stably trapped at the center of this subwavelength dark spot. The refractive index of the air bubble is lower than the ambient medium. The axial and transverse trap distances are 0.62λ and 0.3081λ. The trap distance obtained under two conditions is less than that in the conventional far-field trap system. The single trap system can be used to accurately trap two types of Rayleigh particles with different refractive indices.

Key words: Near-field trapping; Refractive index; Fresnel zone plate; Rayleigh particle; Truncation parameter
OCIS Codes: 050.1960; 140.7010; 350.4855

Foundation item: The National Natural Science Foundation of China (Nos. 61377021, 61078023) and the Public Welfare Project of Zhejiang Province Science and Technology Office (No. 2010C31051)
First author: ZHAO Yan (1990—), female, M. S. degree, mainly focuses on optical trapping. Email: lotus0430@126.com
Responsible author(Corresponding author): ZHANG Yao-ju (1960—), male, professor, Ph. D. degree, mainly focuses on grating, optical trapping and optical storage. Email: zhangyaoju@sohu.com
Received: Feb. 26, 2014; **Accepted**: Apr. 04, 2014

0 Introduction

Since Ashkin successfully accelerated and trapped micrometer-sized neutral particles by radiation pressure from the visible laser light in 1970[1], the optical trapping technique has been widely applied to various fields, such as physics, chemistry and biology. One of the most successful applications in biology is the nondestructive trapping and manipulation of living cells, bacteria and viruses[2-4]. Particles whose refractive index is higher than the ambient (e. g., colloidal gold in water) can be trapped by a bright spot[5-8]. By contrast, particles whose refractive index is lower than the ambient (e. g., cellular vesicles in water) should be trapped by a dark spot[9-10]. Usually, two different optical systems are required for trapping high and low refractive index particles. Recently, some researcher groups have proposed to trap both of these two kinds of particles using a single optical trapping system[11-12].

Though far-field trapping is absolutely accessible to micro-sized particles, it′s difficult to manipulate particles at the nanometer scale due to diffraction limitation. However, near-field trapping is valid to particles in the range from microscale down to nanoscale. In 1992, Kawata and Sugiura experimentally observed the movement of microparticles in the evanescent wave which was produced in the near field of the surface of a prism illuminated by a laser under the total internal reflection condition[13]. The sharp metallic tips[14-15] and nanoapertures[16] can be used to enhance the evanescent field and reduce the trapping volume. Gu et al. reported a focused evanescent wave trapping technique by the use of a ring beam produced by a centrally obstructive objective[17], and both micro- and nano-particles could be easily trapped in three-dimensional (3D) trap form. Recently, more near-field trapping methods have been suggested to trap high-refractive-index micro/nanoparticles[18-21]. Compared with the near-field trap for high-refractive-index particles, to the best of our knowledge, the near-field trap for low-refractive-index particles is seldom considered.

In this paper, we propose a novel method to trap microparticles with high and low refractive index in the near field. In our method, near-field focused 3D bright and dark spots are generated by a binary phase Subwavelength Fresnel Zone Plate (SFZP) under the illumination of double-ring-shaped Laguerre-Gaussian (LG_{10}) vortex beams with the appropriate truncation parameter and vortex angle. We calculate the focusing filed distribution using the diffraction theory of the vectorial angular spectrum and the optical trapping force acting on Rayleigh particles using the Rayleigh scattering theory.

1 The electric and magnetic fields diffracted by the SFZP

Fig. 1(a) shows the section plot of a circular binary phase SFZP. The Fresnel zone plate pattern is etched in the substrate of glass and then it is immersed into water in the right half space. The SFZP is normally illuminated by a LG_{10} beam with the inhomogeneous polarization distribution.

$$\begin{pmatrix} E_{ix}(r,\varphi) \\ E_{iy}(r,\varphi) \end{pmatrix} = AB(r)\begin{pmatrix} \cos(\varphi+\delta) \\ \sin(\varphi+\delta) \end{pmatrix} = AL_1^0\left(2\frac{r^2}{w^2}\right)\exp\left(-\frac{r^2}{w^2}\right)\begin{pmatrix} \cos(\varphi+\delta) \\ \sin(\varphi+\delta) \end{pmatrix} \tag{1}$$

where L_1^0 is the associated Laguerre-Gassuain polynomial with the unit radial node and zero topological charge. w is the beam waist and δ is the vortex angle that denotes the inhomogeneous polarization distribution of the incident beam (see Fig. 1(b)). A is a constant amplitude factor which is related to the power of the incident beam P_0, given by

$$A = \sqrt{\frac{\eta_0 P_0}{\pi\int_0^\infty |B(r)|^2 r\mathrm{d}r}} \tag{2}$$

Here $\eta_0 = (\mu_0/\varepsilon_0)^{1/2}$ is the intrinsic impedance of vacuum. ε_0 and μ_0 are the permittivity and the permeability in vacuum. For the SFZP considered in this paper, we assume the width of the outermost zone is limited between $\lambda/3$ and λ to achieve subwavelength focusing spots[22]. Under this condition, the coupling effect of lights between groove and ridge zones inside the grating′s body can be neglected[23-24] so that the ray optics approximation can be used to calculate the propagating of lights inside the SFZP′s body. When the cylindrical vector vortex beam is normally incident onto the SFZP, the electric field in the exit plane of $z=0$ can be written as

$$\begin{pmatrix} E_{0x}(r,\varphi) \\ E_{0y}(r,\varphi) \end{pmatrix} = AB(r)[t_A C(r) + t_B D(r)\exp(\mathrm{i}kn_m d)]\begin{pmatrix} \cos(\varphi+\delta) \\ \sin(\varphi+\delta) \end{pmatrix} \tag{3}$$

where $k=2\pi/\lambda_0$ is the wave number in vacuum (λ_0 is the wavelength in vacuum). n_m is the refractive index of water. d is the etching depth of the SFZP. t_A and t_B are the Fresnel transmission coefficients of lights passing through the thickness of h and $(h-d)$, respectively. $C(r)$ and $D(r)$ correspond to the structures of the ridge and groove zones of the SFZP, respectively, given by

$$C(r) = \sum_{n=0}^{N}\mathrm{circ}\left(\frac{r}{r_{2n+1}}\right) - \mathrm{circ}\left(\frac{r}{r_{2n}}\right) \tag{4}$$

$$D(r)=\sum_{n=1}^{N}\mathrm{circ}\left(\frac{r}{r_{2n}}\right)-\mathrm{circ}\left(\frac{r}{r_{2n-1}}\right) \tag{5}$$

In Eqs. (4) and (5), $r_j=[j\lambda f+(j\lambda/2)^2]^{1/2}$ is the radius of the jth zone. $\lambda=\lambda_0/n_{\mathrm{m}}$ is the wavelength in water, $2N$ is the number of zones, and f is the designed focal length. The circ denotes the circular function defined as $\mathrm{circ}(r/r_j)=1$ for $r<r_j$ and 0 for $r>r_j$.

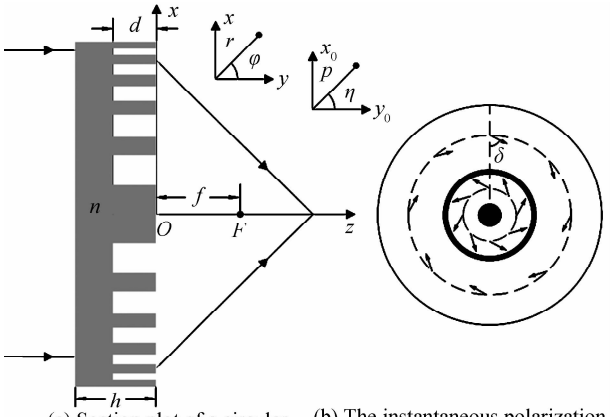

(a) Section plot of a circular binary phase SFZP (b) The instantaneous polarization pattern of doible-ring-shaped beam

Fig. 1 Schematic diagram of the optical trapping setup

After lights pass through the SFZP, we use the angular spectrum method [25] to calculate the diffraction field. The electric field in the half space of $z>0$ can be written in the Cartesian coordinate system as

$$E_x(\rho,\eta,z)=-\frac{1}{(2\pi)^2}\int_0^{\infty}\int_0^{2\pi}A_x(\xi,\varphi)\exp(\mathrm{i}\xi_z z)\times \exp[\mathrm{i}\rho\xi\cos(\varphi-\eta)]\xi\mathrm{d}\xi\mathrm{d}\varphi \tag{6}$$

$$E_y(\rho,\eta,z)=-\frac{1}{(2\pi)^2}\int_0^{\infty}\int_0^{2\pi}A_y(\xi,\varphi)\exp(\mathrm{i}\xi_z z)\times \exp[\mathrm{i}\rho\xi\cos(\varphi-\eta)]\xi\mathrm{d}\xi\mathrm{d}\varphi \tag{7}$$

$$E_z(\rho,\eta,z)=\frac{1}{(2\pi)^2}\int_0^{\infty}\int_0^{2\pi}\frac{\xi_x A_x(\xi,\varphi)+\xi_y A_y(\xi,\varphi)}{\xi_z}\exp(\mathrm{i}\xi_z z)\times\exp[\mathrm{i}\rho\xi\cos(\varphi-\eta)]\xi\mathrm{d}\xi\mathrm{d}\varphi \tag{8}$$

where (ρ,η,z) denotes the observation point in the cylindrical coordinate system. $\xi_z=(k^2-\xi^2)^{1/2}$ is for propagating waves and $\xi_z=\mathrm{i}(\xi^2-k^2)^{1/2}$ is for evanescent waves. A_x and A_y can be obtained from the spatial Fourier transform from E_{0x} and E_{0y} in Eq. (3), given by

$$A_x(\xi,\varphi)=\int_0^{\infty}\int_0^{2\pi}E_{0x}\exp[-\mathrm{i}r\xi\cos(\varphi-\varphi)]r\mathrm{d}r\mathrm{d}\varphi=\mathrm{i}2\pi\cos(\varphi+\delta)T(\xi) \tag{9}$$

$$A_y(\xi,\varphi)=\int_0^{\infty}\int_0^{2\pi}E_{0y}\exp[-\mathrm{i}r\xi\cos(\varphi-\varphi)]r\mathrm{d}r\mathrm{d}\varphi=\mathrm{i}2\pi\sin(\varphi+\delta)T(\xi) \tag{10}$$

with

$$T(\xi)=At_A\sum_{n=0}^{N}\int_{r_{2n}}^{r_{2n+1}}J_1(r\xi)r\mathrm{d}r+At_B\exp(\mathrm{i}kn_m d)\cdot\sum_{n=1}^{N}\int_{r_{2n-1}}^{r_{2n}}J_1(r\xi)r\mathrm{d}r \tag{11}$$

Here J_n is the nth order Bessel function of the first kind. Substituting Eqs. (9)-(11) into Eqs. (6)-(8), the electric field diffracted by the SFZP in the cylindrical coordinate system is obtained as

$$E_\rho(\rho,\eta,z)=\cos\delta\int_0^{\infty}T(\xi)J_1(\rho\xi)\exp(\mathrm{i}\xi_z z)\xi\mathrm{d}\xi \tag{12}$$

$$E_\eta(\rho,\eta,z)=\sin\delta\int_0^{\infty}T(\xi)J_1(\rho\xi)\exp(\mathrm{i}\xi_z z)\xi\mathrm{d}\xi \tag{13}$$

$$E_z(\rho,\eta,z)=i\cos\delta\int_0^{\infty}\frac{\xi^2}{\xi_z}T(\xi)J_0(\rho\xi)\exp(\mathrm{i}\xi_z z)\mathrm{d}\xi \tag{14}$$

Similarly, we obtain the magnetic field in the $z>0$ space, giving

$$H_\rho(\rho,\eta,z)=-\frac{\sin\delta}{\eta_m}\int_0^{\infty}T(\xi)J_1(\rho\xi)\exp(\mathrm{i}\xi_z z)\xi\mathrm{d}\xi \tag{15}$$

$$H_\eta(\rho,\eta,z)=\frac{\cos\delta}{\eta_m}\int_0^{\infty}T(\xi)J_1(\rho\xi)\exp(\mathrm{i}\xi_z z)\xi\mathrm{d}\xi \tag{16}$$

$$H_z(\rho,\eta,z)=-i\frac{\sin\delta}{\eta_m}\int_0^{\infty}\frac{\xi^2}{\xi_z}T(\xi)J_0(\rho\xi)\exp(\mathrm{i}\xi_z z)\mathrm{d}\xi \tag{17}$$

Here $\eta_{\mathrm{m}}=(\mu_0/\varepsilon_{\mathrm{m}})^{1/2}$ is the intrinsic impedance of medium and ε_m is the relative permittivity of the ambient medium.

Fig. 2 shows the electric intensity distributions in the xz plane for different truncation parameters and vortex angles. Calculation parameters are $P_0=300$ mw, $\lambda=0.633$ μm, $f=0.5$ μm, $N=8$ (NA=0.994), $d=1.5028$ μm and $h=1000$ μm, $n_{\mathrm{m}}=1.332$, and $n=1.5426$. When $\beta=1.09$ and $\delta=0$, that is, under the illumination of the radially-polarized LG_{10} beam, the SFZP generates a rotationally symmetric 3D bright spot around the optical axis, and the actual focus is at $z=0.4411\lambda$, as shown in Fig. 2(a). The Depth of Focus (DoF) and the Full-Width-At-Half-Maximum (FWHM) in the actual focal plane are 1.0134λ and 0.3149λ, respectively. Such small a bright spot can be used to trap a microparticle with high refractive index. However, when $\beta=1.45$ and $\delta=0.414\pi$, the SFZP generates a rotationally symmetric 3D dark spot surrounded by a light shell. The center of the dark spot locates at $z=0.7855\lambda$ and its FWHM and DoF sizes are 0.3038λ and 0.5897λ, respectively. Such small a 3D dark spot can be used to three-dimensionally trap a low-refractive-index microparticle. If the uniformity (U) of the light shell surrounding a dark spot is described by the ratio between minimum and maximum peak intensities in the light shell, $U=0.57$ in Fig. 2(b). We find that U decreases when δ deviates from 0.414π (see Figs. 2(c) and 2(d)). When $\delta=0$, there are two separate bright spots in the diffraction field, which could be used to trap two high-refractive-index particles simultaneously. Cartesian coordinates (x_b, z_b) in Fig. 2(a) define positions with respect to the center of the bright spot. The v_b direction in Fig. 2(a) denotes the direction at an angle of 45° with respect to the positive z_b axis in the $x_b z_b$ system. Cartesian coordinates (x_d, z_d) in Fig. 2(b) define positions with respect to the center of the dark spot. The v_d direction in Fig. 2(b) denotes the direction which has the lowest height of the light shell surrounding the dark spot in the $x_d z_d$ system.

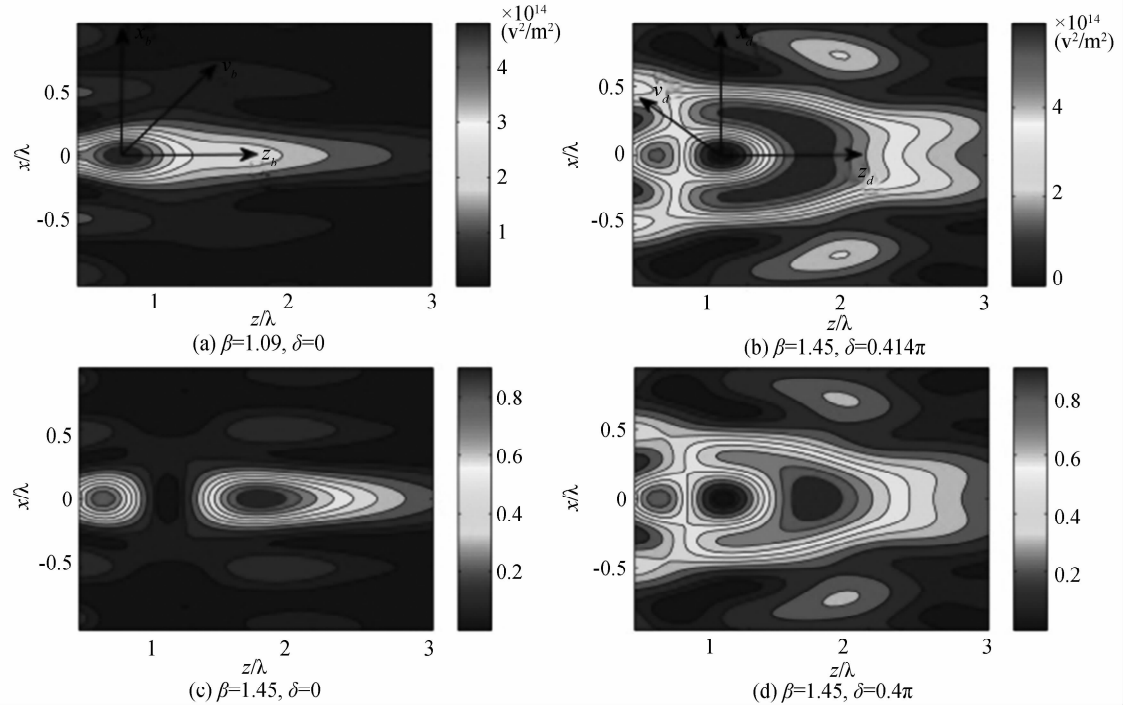

Fig. 2 Total intensity distributions of the electric field in the xz plane

The time averaged Poynting vector is defined as

$$S=\mathrm{Re}(E\times H^{*})/2. \tag{18}$$

Substituting Eqs. (12)-(17) into Eq. (18) we can calculate the distribution of S in the diffraction field generated by the SFZP. Fig. 3 shows the axial component (S_z) of the time averaged Poynting vector. It is noted that S_z is very small in the vicinity of the optical axis and $S_z=0$ on the optical axis. Such axial distribution is very useful for trapping absorptive and/or metal particles. It is found that the scattering distance when $\beta=1.45$ and $\delta=0.414\pi$ is longer than that when $\beta=1.09$ and $\delta=0$.

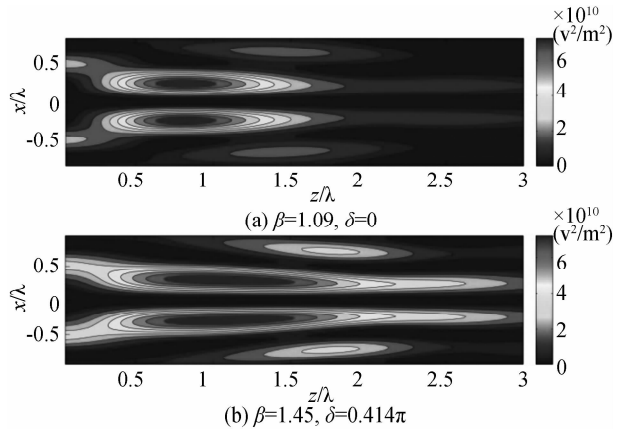

Fig. 3 Axial component of the time averaged Poynting vector in the xz plane

2 Optical trapping forces on Rayleigh particles

A microparticle with refractive index n_p is placed in the vicinity of the actual focus at which the focusing intensity is maximum for a bright trap and minimum for a dark trap. The microparticle can be regarded as a Rayleigh particle with a dipole moment in the diffraction field. According to the Rayleigh scattering theory, radiation forces acting on the microparticle can be evaluated by two components: one is a so-called gradient force, which is essentially due to the Lorentz force acting on the dipole induced by the inhomogeneous electromagnetic field and the other one is a so-called scattering force which is the sum of scattering and absorption forces. The gradient force $\boldsymbol{F}_{\mathrm{grad}}$ is in proportion to the intensity gradient of light and the scattering force $\boldsymbol{F}_{\mathrm{scat}}$ is dependent on the time averaged Poynting vector, which can be expressed as [5]

$$\boldsymbol{F}_{\mathrm{grad}}=\mathrm{Re}(\alpha)\varepsilon_0\ \nabla I/4 \tag{19}$$

$$\boldsymbol{F}_{\mathrm{scat}}=n_m S(C_{\mathrm{scat}}+C_{\mathrm{abs}})/c \tag{20}$$

where $\alpha=4\pi r3\ \mathrm{p}\varepsilon_m(\varepsilon_{\mathrm{p}}-\varepsilon_m)/(\varepsilon_{\mathrm{p}}+2\varepsilon_m)$ is the polarizability of the particle, and r_{p} is the particle radius. ε_{p} is the relative permittivity of the particle. c is the light speed in vacuum. $I=|E|^2$ is the total intensity of the electric field. C_{scat} and C_{abs} are the scattering and absorption cross sections, respectively, given by $C_{\mathrm{scat}}=k4\ 0|\alpha|^2/6\pi$ and $C_{\mathrm{abs}}=k_0 n_m \mathrm{Im}(\alpha)/\varepsilon_m$. From the Fig. 3 it can be noted the axial component of the time averaged Poynting vector makes no contribution to the axial scattering force, that is, $\boldsymbol{F}_{\mathrm{scat}}=0$ on the optical axis.

The 3D trapping occurs at the actual focus where all the components of $\boldsymbol{F}_{\mathrm{grad}}$ vanish with a negative derivative. When the Brownian motion of particle is ignored, the condition of a stable trap is that all the

components of $\boldsymbol{F}_{\mathrm{grad}}$ at the trapping point are larger than that of $\boldsymbol{F}_{\mathrm{scat.}}$ In the following analysis, we present two calculation examples: the first example is to analyze the trapping characteristics for a gold particle (whose refractive index is larger than that of water) using the bright spot in Fig. 2(a) and the second example for a air bubble (whose refractive index is smaller than that of water) using the 3D dark spot in Fig. 2(b).

Fig. 4 shows that the distribution of radiation forces acting on a gold particle in the z_b, x_b and v_b directions, respectively. The radius of the gold particle is $r_p = 19.1$ nm and its relative permittivity is $\varepsilon_p = -9.5+1.2\mathrm{i}$. Comparison shows that the scattering force is much smaller than that of the corresponding gradient force. In the special case on the optical axis, $\boldsymbol{F}_{\mathrm{scat}} = 0$ as predicted in the above section, and the

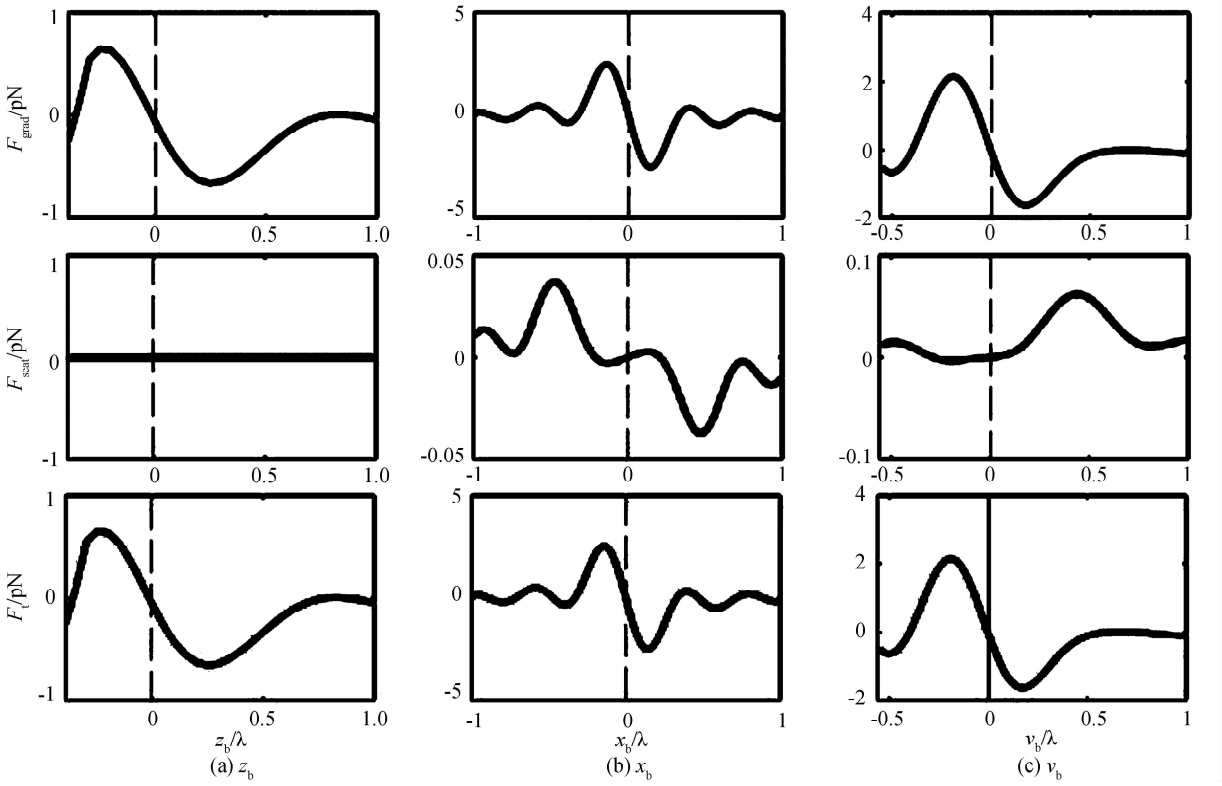

Fig. 4 Radiation forces on a gold particle in the z_b, x_b and v_b directions

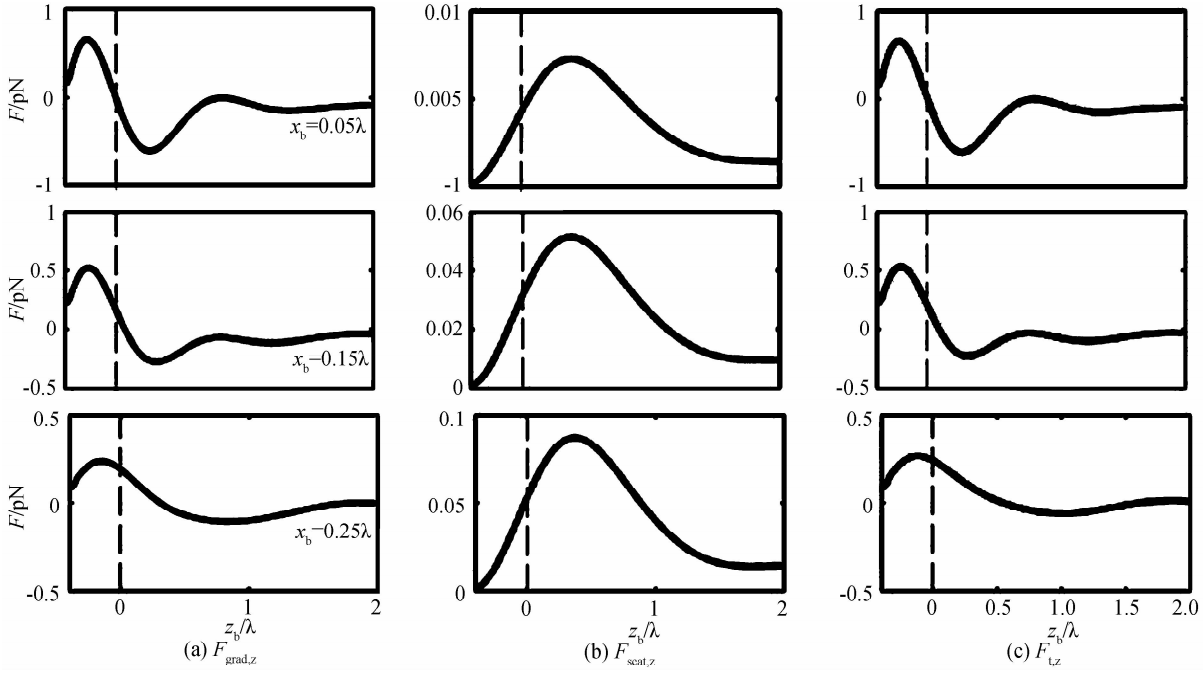

Fig. 5 The axial gradient force, the axial scattering force, and the total axial trapping force on a gold particle for three different off-axis distances of $x_b = 0.05\lambda$, 0.15λ, and 0.25λ

equilibrium position locates at the center of the bright spot ($z_{b,equ}=0$). If the distance between positive and negative peak values of the total trapping force ($\boldsymbol{F}_t=\boldsymbol{F}_{grad}+\boldsymbol{F}_{scat}$) is defined as the trap distance, both the axial trap distance (0.4921λ) and the transverse trap distance (0.2844λ) are small enough to provide an accurate trap in the near field. The subwavelength trap distance we obtained is much smaller than that obtained by far-filed trap systems [7,12]. When the particle is at off-axis position, the axial scattering force is no longer zero and the axial equilibrium position shifts to the forward propagation direction. The shift of the equilibrium position is larger and the maximum gradient force is smaller for the larger off-axis distance, as shown in Fig. 5. If $k_z=|\partial F_{t,z}/\partial z_b|_{z_b,equ}$ is defined as the axial trap stiffness, where $F_{t,z}$ is the total axial trapping force, k_z decreases as the off-axis distance x_b increases. These results imply that the gold particle is easier to be trapped into the bright spot for small off-axis distances. For larger off-axis distance, for example, $x_b>0.25\lambda$, the particle cannot be effectively trapped.

Fig. 6 shows that the distribution of radiation forces acting on an air bubble of $r_p=30$ nm and $\varepsilon_p=1$ using the 3D dark spot in Fig. 2(b). It is found that the gradient force is much larger than the scattering force in this dark trap and the air bubble can be trapped at the actual focus. The peak value of the gradient force is maximum along the radial axis ($F_{grad,max}=0.1101$ pN) and is minimum along the optical axis ($F_{grad,min}=0.0485$ pN). The axial trap distance (0.62λ) and the transverse trap distance (0.3081λ) are also smaller than that of far-field trap systems. It is noted that the gradient force of the 3D dark spot trap is ten times smaller than that of the bright spot trap in the first example.

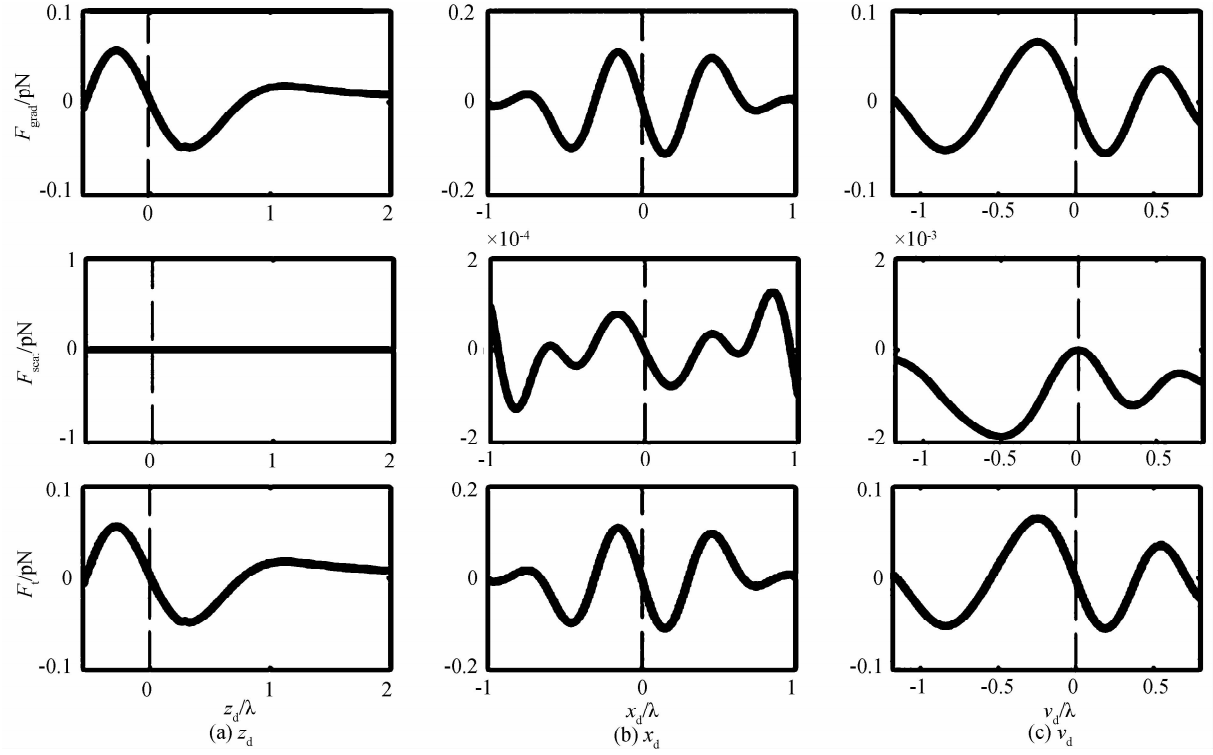

Fig. 6 Radiation forces on an air bubble in the z_d, x_d and v_d directions

3 Trapping stabilities

To stably 3D trap a Rayleigh particle, two stability conditions [5,26] need to be satisfied. One is that gradient force must be opposite to the propagation direction, *i. e.*, $R=\boldsymbol{F}_{grad}/\boldsymbol{F}_{scat}>1$, where R is the stability criterion. Considering the asymmetrical distribution of the axial gradient force, a more conservative estimation here can be written as $R=\min\{(F^p\ \mathrm{grad})_{max},(F^n\ \mathrm{grad})_{max}\}/|F_{scat}|_{max}>1$, where $(F^p\ \mathrm{grad})_{max}$ and $(F^n\ \mathrm{grad})_{max}$ are the maximum values in the positive and negative gradient force directions. The function $\min\{A,B\}$ means to take the smaller one between A and B. After several calculations, the values of R are 26.8 for the gold particle in the v_b direction and 29.1 for the air bubble in the v_d direction, respectively. Another necessary and sufficient condition is that the potential well generated by gradient forces must be deep enough to overcome the kinetic energy in the Brownian motion. The criterion is $R_{Thermal}=e^{-U_{max}/kBT}<1$, where U_{max} is the potential depth given by $U_{max}=|\mathrm{Re}(\alpha)\varepsilon_0 I_{max}/4|$. Under a temperature of $T=300$ K, the values of $R_{Thermal}$ come out to be 2.16×10^{-36} for the gold particle and 0.1278 for the air

bubble, separately. The results calculated above demonstrate particles with high and low refractive index can be stably trapped by giving the appropriate truncation parameter and the vortex angle.

4 Conclusions

We′ve proposed a method of near-field trapping high and low refractive index particles using a single optical system. In our method, a SFZP under the illumination of a double-ring-shaped LG_{10} vortex beam is used to generate bright and dark spots. The calculations based on the vector angular spectrum theory show that, by simply adjusting the truncation parameter and vortex angle, the proposed system can generate tiny three-dimensional bright and dark spots in the near-field region. The tiny 3D bright spot can trap high-refractive-index microparticles and the tiny 3D dark spot can trap low-refractive-index microparticles. We present two examples of numerical calculations: one is the use of the generated tiny 3D bright spot to trap a Rayleigh gold particle whose refractive index is larger than that of the ambient and another is the use of the generated tiny 3D dark spot to trap a small air bubble whose refractive index is smaller than that of the ambient. Numerical results show that when $\beta=1.09$ and $\delta=0$ the Rayleigh gold particle can be stably trapped and when $\beta=1.45$ and $\delta=0.414\pi$ the small air bubble can be stably trapped. The obtained axial trap distance is shorter than that of the far-field trap system, which implies that the accuracy of the proposed near-field trap system is higher. It is noted that the stability of the dark trap is lower than that of the bright spot. But this disadvantage could be overcome by optimizing the structure of the SFZP, which will be studied in the future.

References

[1] ASHKIN A. Acceleration and trapping of particles by radiation pressure[J]. *Physical Review Letters*, 1970, **24**(4): 156-159.

[2] ASHKIN A, DZIEDZIC J M. Optical trapping and manipulation of viruses and bacteria[J]. *Science*, 1987, **20**(4795): 1517-1520.

[3] KAUPPILA A, KINNUNEN M, KARMENYAN A. *et al*. Measurement of the trapping efficiency of an elliptical optical trap with rigid and elastic objects[J]. *Applied Optics*, 2012, **51**(23): 5705-5712.

[4] LIU T H, XIAO Jian-hong, LEE C H, *et al*. Measurement of membrane rigidity on trapped unilamellar phospholipid vesicles by using differential confocal microscopy[J]. *Applied Optics*, 2011, **50**(19): 3311-3315.

[5] HARADA Y, ASAKURA T. Radiation forces on a dielectric sphere in the Rayleigh scattering regime [J]. *Optics Communications*, 1996, **124**(5-6): 529-541.

[6] ZHAN Qi-wen. Trapping metallic Rayleigh particles with radial polarization[J]. *Optics Express*, 2004, **12**(15): 3377-3382.

[7] ZHANG Yao-ju, SUYAMA T, DING Biao-feng. Longer axial trap distance and larger radial trap stiffness using a double-ring radially polarized beam[J]. *Optics Letters*, 2010, **35**(8): 1281-1283.

[8] LIU Zhi-rong, ZHAO Dao-mu. Optical trapping Rayleigh dielectric spheres with focused anomalous hollow beams[J]. *Applied Optics*, 2013, **52**(6): 1310-1316.

[9] PRENTICE P, MACDONALD M, FRANK T, *et al*. Manipulation and filtration of low index particles with holographic Laguerre-Gaussian optical trap arrays[J]. *Optics Express*, 2004, **12**(4): 593-600.

[10] PENG Fei, YAO Bao-li, YAN Shao-hui, *et al*. Trapping of low-refractive-index particles with azimuthally polarized beam [J]. *Journal of the Optical Society of America B*, 2009, **26**(12): 2242-2247.

[11] ZHAO Cheng-liang, WANG Li-gang, LU Xuan-hui. Radiation forces on a dielectric sphere produced by highly focused hollow Gaussian beams[J]. *Physics Letters A*, 2007, **363**(5-6): 502-506.

[12] ZHANG Yao-ju, DING Biao-feng, SUYAMA T. Trapping two types of particles using a double-ring-shaped radially polarized beam[J]. *Physical Review A*, 2010, **81**(2): 023831.

[13] KAWATA S, SUGIURA T. Movement of micrometer-sized particles in the evanescent field of a laser beam[J]. *Optics Letters*, 1992, **17**(11): 772-774.

[14] NOVOTNY L, BIAN R X, XIE X S. Theory of Nanometric Optical Tweezers[J]. *Physical Review Letters*, 1997, **79**(4): 645-648.

[15] CHAUMET P C, RAHMANI A, NIETO-VESPERINAS M. Optical trapping and manipulation of nano-objects with an apertureless probe[J]. *Physical Review Letters*, 2002, **88**(12): 123601.

[16] OKAMOTO K, KAWATA S. Radiation force exerted on subwavelength particles near a nanoaperture[J]. *Physical Review Letters*, 1999, **83**(22): 4534-4537.

[17] GU M, HAUMONTE J B, MICHEAU Y, *et al*. Laser trapping and manipulation under focused evanescent wave illumination[J]. *Applied Physics Letters*, 2004, **84**(21): 4236-4238.

[18] RIGHINI M, GHENUCHE P, CHERUKULAPPURATH S, *et al*. Nano-optical trapping of Rayleigh particles and Escherichia coli bacteria with resonant optical antennas [J]. *Nano Letters*, 2009, **9**(10): 3387-3391.

[19] YANG A H J, MOORE S D, SCHMIDT B S, *et al*. Optical manipulation of nanoparticles and biomolecules in sub-wavelength slot waveguides[J]. *Nature*, 2009, **457**(7225): 71-75.

[20] ZHANG Wei-hua, HUANG Li-na, SANTSCHI C, *et al*. Trapping and sensing 10 nm metal nanoparticles using plasmonic dipole antennas[J]. *Nano Letters*, 2010, **10**(3): 1006-1011.

[21] PANG Yuan-jie, GORDON R. Optical trapping of 12 nm dielectric spheres using double-nanoholes in a gold film[J]. *Nano Letters*, 2011, **11**(9): 3763-3767.

[22] MOTE R G, YU S F, ZHOU W, *et al*. Subwavelength focusing behavior of high numerical-aperture phase Fresnel zone plates under various polarization states[J]. *Applied Physics Letters*, 2009, **95**(19): 191113.

[23] CHEN Qin. A novel plasmonic zone plate lens based on nano-slits with refractive index modulation[J]. *Plasmonics*, 2011, **6**(2): 381-385.

[24] HU Bin, WANG Qi-jie, ZHANG Ying. Systematic study of the focal shift effect in planar plasmonic slit lenses [J]. *Nanotechnology*, 2012, **23**(44): 444002.

[25] HELSETH L E. Radiationless electromagnetic interference shaping of evanescent cylindrical vector waves[J]. *Physical Review A*, 2008, **78**(1): 013819.

[26] ASHKIN A, DZIEDZIC J M, BJORKHOLM J E, *et al*. Observation of a single-beam gradient force optical trap for dielectric particles[J]. *Optics Letters*, 1986, **11**(5): 288-290.